

## **Effective Strain of RC Beams Strengthened in Shear with FRP**

### Author

Lee, Jung-Yoon, Hwang, Hyun-Bok, Doh, Jeung-Hwan

### Published

2012

### Journal Title

Composites Part B: Engineering

### DOI

[10.1016/j.compositesb.2011.11.050](https://doi.org/10.1016/j.compositesb.2011.11.050)

### Rights statement

© 2011 Elsevier. This is the author-manuscript version of this paper. Reproduced in accordance with the copyright policy of the publisher. Please refer to the journal's website for access to the definitive, published version.

### Downloaded from

<http://hdl.handle.net/10072/42415>

### Griffith Research Online

<https://research-repository.griffith.edu.au>

## Accepted Manuscript

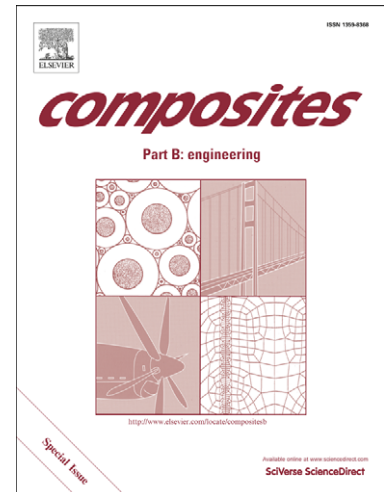
Effective Strain of RC Beams Strengthened in Shear with FRP

Jung-Yoon Lee, Hyun-Bok Hwang, Jeung-Hwan Doh

PII: S1359-8368(11)00519-1  
DOI: [10.1016/j.compositesb.2011.11.050](https://doi.org/10.1016/j.compositesb.2011.11.050)  
Reference: JCOMB 1598

To appear in: *Composites: Part B*

Received Date: 29 October 2010  
Revised Date: 19 July 2011  
Accepted Date: 30 November 2011



Please cite this article as: Lee, J-Y., Hwang, H-B., Doh, J-H., Effective Strain of RC Beams Strengthened in Shear with FRP, *Composites: Part B* (2011), doi: [10.1016/j.compositesb.2011.11.050](https://doi.org/10.1016/j.compositesb.2011.11.050)

This is a PDF file of an unedited manuscript that has been accepted for publication. As a service to our customers we are providing this early version of the manuscript. The manuscript will undergo copyediting, typesetting, and review of the resulting proof before it is published in its final form. Please note that during the production process errors may be discovered which could affect the content, and all legal disclaimers that apply to the journal pertain.

## Effective Strain of RC Beams Strengthened in Shear with FRP

Jung-Yoon Lee<sup>a</sup>, Hyun-Bok Hwang<sup>a</sup> and Jeung-Hwan Doh<sup>b\*</sup>

<sup>a</sup>*Department of Civil, Architectural and Environmental System Engineering, Sungkyunkwan University, Suwon, Republic of Korea*

<sup>b</sup>*Griffith School of Engineering, Griffith University Gold Coast Campus, Queensland 4222, Australia (corresponding author, email: j.doh@griffith.edu.au)*

### ABSTRACT

The failure modes of reinforced concrete (RC) beams strengthened in shear with fiber reinforced polymer (FRP) sheets or strips are not well understood as much as those of RC beams reinforced with steel stirrups. When the beams are strengthened in shear with FRP composites, beams may fail due to crushing of the concrete before the FRP reaches its rupture strain. Therefore, the effective strain of the FRP plays an important role in predicting the shear strength of such beams. This paper presents the results of an analytical and experimental study on the performance of reinforced concrete beams strengthened in shear with FRP composites and internally reinforced with conventional steel stirrups. Ten RC beams strengthened with varying FRP reinforcement ratio, the type of fiber material (carbon or glass) and configuration (continuous sheets or strips) were tested. Comparisons between the observed and calculated effective strains of the FRP in the tested beams failing in shear showed reasonable agreement.

**Keywords:** A. Polymer Fibre; B. Strength; B. Mechanical Properties; D. Mechanical Testing.

---

\*Corresponding author. Tel.: +61 7 5552 9141; Fax: +61 7 5552 8065.

E-mail address: j.doh@griffith.edu.au (J.-H. Doh).

## 1. Introduction

Fiber Reinforced Polymer (FRP) is a relatively new class of composite material manufactured from fibers and resins and has proven efficient and economical for the development and repair of deteriorating structures in civil engineering.

The strength of FRP-strengthened RC members is influenced by the type of fibers, fiber directions, fiber distributions, and bond schemes. The effectiveness of FRP is maximized by bonding the external FRP reinforcement parallel to the direction of principal tensile stress.

FRP bond schemes (e.g. side bonding, U jacketing, wrapping) can also result in different shear capacity of FRP-strengthened RC members. Detailed investigations on the shear strengthening of RC members have been relatively limited, and many questions regarding the strengthening mechanism are yet to be resolved. With a few exceptions, most researchers have idealized the FRP materials as being analogous to internal steel stirrups, assuming that the contribution of FRP to shear capacity emanates from the capacity of the fibers to carry tensile stresses at a more or less constant strain, which is equal to or lower than the FRP ultimate tensile strain. Current national code provisions are available for designing elements externally bonded with FRP, and many experimental tests have been carried out in this field of research.

Both experimental evidences and code suggestions indicate that a performance improvement can be realized, but even if a lot of solutions are possible, their performances and beneficial effects are not yet quantified [1].

Table 1 shows various equations (see Eq. 1 to 5) developed by others to estimate the effective strain of FRP ( $\varepsilon_{fe}$ ) at shear failure. Recently, Teng *et al.* [2] tested nine FRP-strengthened RC beams: three as control specimens, three with bonded FRP full wraps, and three with FRP full wraps left unbonded to the beam sides. The test results showed that the unbonded FRP wraps had a slightly higher shear strength capacity than the bonded FRP wraps. In addition, Deifalla and Ghobarah [3] tested six half-scale beams externally bonded with FRP composites constructed using a specially designed test setup in order to investigate the strengthening techniques for beams subjected to combined shear and torsion. Test results indicated that externally bonded CFRP strengthening schemes enhanced the shear and torsion carrying capacities of RC beams. Grande *et al.* [4] tested fifteen RC beams strengthened in shear by externally bonded fiber-reinforced plastics (FRP) sheets to study the influence that the geometrical percentage of transverse steel reinforcement could had on the FRP resisting action. The experimental investigation indicated the variability of the FRP shear resisting action over the amount of the transverse steel reinforcement. In particular, the FRP shear resisting action was generally smaller in beams with closer stirrups. Fico *et al.* [5] studied the assessment of Eurocode design equations for the evaluation of the shear strength of FRP RC members, as proposed by the guidelines of the Italian Research Council. Li *et al.* [6] tested sixteen RC beams with or without FRP composites to study the shear strengthening effect. The experimental results indicated that the shear contribution of FRP composites was

influenced by the applied FRP composite area, the spacing between the steel stirrups, and the longitudinal steel bar diameter of the RC beams. Although there are many proposed equations to determine  $\varepsilon_{fe}$ , it is generally agreed that the effective strain of FRP is difficult to predict solely by rigorous analysis because  $\varepsilon_{fe}$  is influenced not only by material properties but also by the shear failure modes of strengthened RC members.

This research aims to investigate the effective shear strain of the FRP used as shear strengthening material in beams that show two different shear failure modes. Included in the study are the stresses and strains of concrete, steel stirrup, and FRP at shear failure.

## **2. Research significance**

The shear failure modes of FRP strengthened concrete beams are quite different from those of the beams strengthened with steel stirrups. This paper presents the results of an experimental and analytical study on the performance of reinforced concrete beams externally wrapped with FRP composites and internally reinforced with steel stirrups. In this investigation, emphasis was placed on the effective strain of the materials (concrete, FRP, and steel bars) of the FRP shear strengthened RC beams at peak load (ultimate stage).

## **3. Effective strain of the FRP**

### *3.1 Failure modes of RC beams shear-strengthened with FRP composites*

The failure modes of RC beams shear-strengthened with FRP composites are more complex than those of RC beams reinforced with conventional steel stirrups. Debonding of FRP composites or concrete crushing, before yielding of the steel stirrups, cause brittle failure. On the other hand, concrete crushing or FRP rupture, after yielding of the steel stirrups, cause ductile failure modes. In this paper, we define the two latter failure modes as:

- **Failure mode 1:** concrete crushing after yielding of the steel stirrups.
- **Failure mode 2:** rupture of FRP composites after yielding of the steel stirrups without concrete crushing.

For the beams showing failure mode 1, the shear resistance contribution of FRP ( $V_f$ ) should be calculated by using the effective strain of FRP ( $\varepsilon_{fe}$ ), because the stress of the FRP at shear failure does not reach its rupture strength ( $f_{fr}$ ). However, for the beams exhibiting failure mode 2, the stress of the FRP at shear failure can be replaced by its rupture strength. FRP debonding failure is one of the main failure modes for RC beams strengthened in shear with externally bonded FRP. The separate treatment of FRP debonding and FRP rupture is essential to develop accurate shear strength models because the failure mechanism of FRP debonding is quite different from that of FRP rupture [10]. This paper placed emphasis on presenting a model to predict the effective strain of RC beams shear strengthened with FRP wraps failing in Failure mode 1 or 2 without debonding.

### 3.2 FRP ratio at the balanced shear failure

The following is the most widely used expression to calculate the shear capacity of FRP-strengthened RC beams,  $V_n$ :

$$V_n = V_c + V_s + V_f \quad (1)$$

where  $V_c$ ,  $V_s$ , and  $V_f$  are the shear resistance contributions of concrete, steel stirrups, and FRP, respectively. Based on the truss model, the shear resistance contribution of FRP can be derived as follow,

$$V_f = \varepsilon_{fe} E_f \rho_f b_w d (\cot \theta + \cot \alpha) \sin \alpha \quad (2)$$

where  $\varepsilon_{fe}$  is the effective strain of FRP when a RC member reaches its shear capacity;  $E_f$  is the elastic modulus of FRP;  $\rho_f$  is the FRP reinforcement ratio;  $b_w$  is the minimum width of cross section;  $d$  is the effective depth of cross section;  $\theta$  is the diagonal crack angle; and  $\alpha$  is the angle between principal fiber orientation and longitudinal axis of the member.

As indicated by the test results in the literatures, the strain distributions of the FRP composites were not uniform and the strain concentrations occurred near the locations of diagonal cracks. In this study, the assumption of continuous material was applied to the compatibility aided truss model to get the effective strain of FRP because the stress (or strain) distributions of the FRP composites are not uniform. Thus, all the stresses and strains involved in this model are the average (or smeared) stresses and average (or smeared) strains.

The effective strain of the FRP at shear failure was related to the amount of shear

reinforcement and the failure mode. In this paper, the effective strain of the FRP at shear failure was formulated starting with the FRP reinforcement ratio corresponding to a balanced shear failure. Fig. 1 shows the stress conditions of the FRP strengthened RC beams after the formation of diagonal cracks. Based on the well-known variable-angle truss models in which the angle  $\theta$  of the cracks in concrete is assumed to be equal to the angle of the principal compressive stress of concrete, the tensile force  $\rho_{tv}f_{tv}$  in the stirrup must counteract the vertical component of the diagonal compressive strut under the equilibrium conditions, and the required FRP reinforcement ratio can be estimated as:

$$\rho_f = \frac{1}{f_f \sin \alpha} (-f_2 \sin^2 \theta - f_1 \cos^2 \theta - \rho_{tv} f_{tv}) \quad (3)$$

where  $f_1$  and  $f_2$  are the principal tensile and compressive stresses of concrete, respectively;  $\rho_{tv}$  and  $\rho_f$  are the steel ratio in the transverse direction and the FRP ratio, respectively;  $f_{tv}$  and  $f_f$  are the steel stress in the transverse direction and the stress of the FRP, respectively.

Fig. 2 shows two typical examples of beam responses up to failure. The horizontal axis indicates the shear strain. The vertical axis in the upper direction indicates stress of the FRP composites and stress of the steel bars, while the vertical axis in the lower direction indicates principal compressive stress of concrete ( $f_2$ ) and the effective compressive strength of concrete ( $\nu f_c'$ ). For the beams with the majority of FRP composites showing failure mode 1, the concrete crushes before the stress of the FRP reaches its rupture strength ( $f_f < f_{fr}$  and

$f_2 = v f_c'$ ), while for the beams with smaller amount of FRP composites showing failure mode 2, the FRP ruptures before concrete crushing ( $f_f = f_{fr}$  and  $f_2 < v f_c'$ ). The boundary between Failure mode 1 and 2 represents the balanced shear failure in which the concrete crushes at the same time as the FRP reaches its rupture strength after the steel stirrups yielded. In the balanced shear failure mode, the principal compressive stress of concrete  $f_2$  in Eq. (3) must equal the effective compressive strength of concrete  $v f_c'$ , and the tensile stresses  $f_{tv}$  and  $f_f$  must be equal to the yield strength  $f_{ty}$  and the rupture strength  $f_{fr}$ , respectively.

Fig. 3 shows the Mohr's stress and strain circles at the boundary between failure mode 1 and failure mode 2. The principal tensile stress of concrete  $f_1$  is ignored because it is much smaller than the other strengths  $v f_c'$ ,  $f_{ty}$ , and  $f_{fr}$ . Therefore, the FRP ratio ( $\rho_{fb}$ ) at the balanced shear failure can be formulated as:

$$\rho_{fb} = \frac{1}{f_{fr} \sin \alpha} (-v f_c' \sin^2 \theta - \rho_{ty} f_{ty}) \quad (4)$$

where  $\rho_{fb}$  is the FRP reinforcement ratio required for a balanced shear failure.

The angle  $\theta$  of the diagonal cracks in Eq. (4) can be determined using Mohr's strain circle as shown in Fig. 3(c).  $\varepsilon_l$  and  $\varepsilon_t$  are the normal strains in the longitudinal and transverse directions;  $\varepsilon_1$  and  $\varepsilon_2$  are the strains of concrete in the principal tension and compression directions, and  $\gamma$  is the shear strain. Thus, the angle  $\theta$  can be expressed in terms of the strains as:

$$\cos \theta = \sqrt{(\varepsilon_t) / (\varepsilon_l + \varepsilon_t - \varepsilon_2)} \quad (5)$$

At the balanced shear failure, the strains of the steel stirrups and the FRP are equal to the rupture strain  $\varepsilon_{fr}$  of the FRP. In addition, because the principal compressive strain of concrete  $\varepsilon_2$  is much smaller than  $\varepsilon_{fr}$  and  $\varepsilon_l$ , the principal compressive strain of concrete can be ignored in Eq. (5) resulting in the following equation:

$$\cos \theta = \sqrt{(\varepsilon_{fr}) / (\varepsilon_l + \varepsilon_{fr})} \quad (6)$$

Several equations [11-14] gave the constitutive relationships of cracked concrete in the principal compressive and tensile directions of concrete. In this study, the effective compressive strength of concrete proposed by Collins *et al.*<sup>7)</sup> will be adopted as below:

$$vf_c' = \frac{1}{0.8 + 170(\varepsilon_l + \varepsilon_{fr})} f_c' \quad (7)$$

The effective compressive strength coefficient of concrete  $v$  of Eq. (7) was originally formulated to predict the shear strengths as well as the deformations of RC membrane elements, such as panels, subjected to shear and normal loads. The equation was also utilized to predict the shear behavior of RC beams [16, 17].

The equilibrium conditions for the longitudinal stresses must satisfy the following Eq. (8):

$$0 = f_2 \cos^2 \theta + f_1 (1 - \cos^2 \theta) + \rho_l E_s \varepsilon_l + \rho_f f_{fr} \cos \alpha \quad (8)$$

By substituting Eq. (6) into Eq. (8) and assuming that  $\varepsilon_2 = f_1 = 0$  for the reasons mentioned earlier, the strain of the tensile longitudinal steel bars  $\varepsilon_l$  can be obtained using Eq. (9):

$$\frac{\varepsilon_{fr}}{\varepsilon_l + \varepsilon_{fr}} (vf_c') + \rho_l E_s \varepsilon_l + \rho_f f_{fr} \cos \alpha = 0 \quad (9)$$

The FRP balanced shear reinforcement  $\rho_{fb} f_{fr}$  was calculated by substituting  $vf_c'$  and

$\theta$  in Eq. (4). The FRP balanced shear ratio vs. the compressive strength of concrete curves for a RC beam calculated using Eq.(4). It is noted that the balanced shear ratio of the FRP  $\rho_{fb}$  increases as the compressive strength of concrete  $f_c'$  increases. This is because as the rupture strain of FRP increases, the strain of concrete in the principal tension direction  $\varepsilon_1$  increases. Accordingly, the  $\rho_{fb}$  is correspondingly reduced due to the decrease in the effective compressive strength of concrete  $v f_c'$  that decreases with the increase of  $\varepsilon_1$ .

### 3.3 Calculation of the effective strain of the FRP

As mentioned in the early part of this paper, for the beams showing failure mode 1, the concrete crushes before the stress of the FRP reaches its rupture strength. Therefore, the effective strain of FRP at shear failure can now be determined by replacing  $\rho_{fb} f_{fr}$  with  $\rho_f f_f (= \rho_f E_f \varepsilon_f)$  in Eq. (4).

For the failure mode 1 beams,

$$\varepsilon_{fe} \rho_f E_f \sin \alpha = (-v f_c' \sin^2 \theta - \rho_{tv} f_{tv}) \quad (\rho_f \geq \rho_{fb}) \quad (10a)$$

For the failure mode 2 beams,

$$\varepsilon_{fe} = \varepsilon_{fr} \quad (\rho_f < \rho_{fb}) \quad (10b)$$

In Eq.(10a),  $v f_c'$  and  $\theta$  can be calculated by replacing  $\varepsilon_{fr}$  with  $\varepsilon_f$  in Eqs. (7) and (6), respectively. The amount of the FRP vs. the strain of the FRP curves for a RC beam are shown in Fig. 4 in which the solid line represents the FRP reinforcement  $\rho_f f_f$ , calculated

using the right term of Eq.(10a), while the dotted line calculated using the left term of Eq. (10a) that linearly increases as the strain of the FRP ( $\varepsilon_f$ ) increases. The intersecting point where two lines cross is the effective strain of FRP at shear failure calculated by Eq.(10a).

In case of a beam having balanced shear FRP ratio  $\rho_{fb}$  and  $f_c' = 40MPa$  (Beam 1,  $\rho_f = \rho_{fb} = 0.000244$ ,  $f_{fr} = 3,825MPa$ ,  $\varepsilon_{fr} = 0.0153$ ,  $E_f = 250GPa$ ,  $\beta = 90^\circ$ ), two lines cross at point A where the calculated strain is 0.0153 that is the rupture strain of the FRP. If the beam is strengthened with a great amount of the FRP than required for the balanced shear failure, say  $\rho_f = 0.0008$ , the slope of the dotted line increases and the effective strain of the FRP  $\varepsilon_{fe}$ , becomes 0.01 of the value at point B (Beam 2). Therefore, this beam fails due to crushing of the concrete before the FRP reaches its rupture strain because the effective strain of 0.01 at point "B" is smaller than the rupture strain  $\varepsilon_{fr} = 0.0153$ . Similarly, if the FRP reinforcement ratio  $\rho_f$  becomes 0.0016, the calculated effective strain of the FRP  $\varepsilon_{fe}$ , decreases to  $\varepsilon_f = 0.0077$  of point "C" as shown in Fig. 4 (Beam 3). It is noted that the effective strain of the FRP  $\varepsilon_{fe}$  decreases as the FRP reinforcement ratio  $\rho_f$  increases for the equilibrium of compressive force of concrete and tension force of FRP composites. The material properties and analytical results of these three example beams are listed in Table 2.

To be able to define the shear strength of RC beams, the effective compressive strength coefficient of concrete  $\nu$ , the normal strain in longitudinal direction  $\varepsilon_l$ , and the angle  $\theta$  of the diagonal cracks should be calculated from Eqs. (6), (7), and (9), respectively. This will

then allow the effective strain of the FRP,  $\varepsilon_{fe}$ , to be determined using Eq. (10). Eq. (2) is then used to calculate the shear resistance contributions of FRP,  $V_f$ .

#### 4. Test program and measurements

##### 4.1. Test specimens

A total of 10 RC beams with the same cross-sectional dimensions were strengthened by FRP-wrap and tested to investigate the effectiveness of FRP at shear failure in detail. The proposed equation (10) is applicable to predict the effective strain of the FRP in RC beams that fail due to crushing of the concrete or FRP rupture without debonding (or premature failure/ peeling off). Therefore the test beams were strengthened by FRP wrapping and designed to prevent debonding failure. The overall dimensions, arrangement of reinforcement, and loading system are shown in Fig. 5. Three parameters were considered in this investigation: FRP reinforcement ratio, the type of fiber materials (carbon “C” or glass “G”) and configuration (continuous sheets “C” or strips “S”). All beams were reinforced with ten bottom 25.4mm steel bars (D25 steel bar) and five top 25.4mm steel bars. The longitudinal tensile reinforcement ratio of all beams was 0.0367. The shear reinforcement consisted of 9.53mm steel stirrups (D10 steel bar) spaced each 200mm. The ratio of steel stirrups was 0.00204. The yield strengths of D25 and D10 steel bars were 524.5 MPa and 300.0 MPa, respectively. All beams were designed to share the same shear span-to-depth ratio ( $a/d=3$ ).

The specimens were cast in formworks of which four corners were rounded at radius of 10mm. These round corners were necessary to alleviate stress concentration which causes premature failure of the external FRP. The beams were removed from the forms after 72 hours. The beams were cured at room temperature for a sufficient period. After curing the beams, the surfaces of the specimens were cleaned using an electric grinder, and primer was applied to the surfaces of the beams. The FRP sheets were then placed using the epoxy (Epondex by Hankuk Carbon Co. Ltd.) after the primer had completely dried.

One concrete batch was used to cast all the beams at the same time. Concrete cylinders were tested on the first and the last day of beam testing. Each test consisted of three cylinders. The average concrete strength of the two cylinder tests was 35.0MPa. Specifications of specimens are given in Table 3. Mechanical properties of the FRP composites and the longitudinal steel rebars used in this investigation are shown in Table 4.

#### *4.2. Loading system and measurements*

The specimens were simply supported and were subjected to a concentrated load at mid-span. Electrical strain gages were installed on the surfaces of the steel bars and FRP sheets to record the strains during the test, as shown in Fig. 5. Because the strain gages can measure only one point strain of stirrups or FRP sheets, five linear displacement transducers (LVDTs) were attached to each face of the beam near the shear critical region to measure the

longitudinal, transverse, and shear average strains of each region. It is noted that the effective strain in Eq.(10) is not the maximum strain but the average strain derived from the compatibility aided truss model. An additional LVDT was placed under the beam at mid-span to measure the deflection of the beam.

## 5. Test Results

All beams failed in shear before flexural yielding, except beam C2 which failed in shear after flexural yielding. Premature failure due to local fracture or debonding of the FRP did not occur in any of the specimens. In the beams strengthened with FRP sheets (beams in C- or G-series), obvious diagonal cracks were not observed at a lower load level because of the presence of the FRP sheets. As the applied load increased, part of the FRP close to the diagonal cracks was torn apart, producing noise. In some specimens, partial debonding of the FRP occurred near the critical shear crack or on the edge of the beam though, eventual failure occurred due to crushing of the concrete. At onset of the concrete failure, strain measurements by strain gages and LVDTs indicated that the FRP did not reach its full tensile capacity.

### 5.1. Load-deflection curves

The beams strengthened with glass-FRP strips showed flexural cracks near the bottom surface of the beam close to mid-span. The formation of these cracks was also reflected in the

load-deflection curve as a sudden reduction in the stiffness of beams. The test results including the shear strength of the beam and the failure modes are shown in Table 3.

The load-deflection curves of the 10 RC beams are presented in Figs. 6 (a) through (e). The strengths of the beams increase with an increasing amount of FRP sheets and strips. Enhanced behaviors of FRP strengthened beams are not only observed in the strength but also in the deflection corresponding to the peak load, leading to higher energy dissipation capacity. As an example, the peak load and the corresponding deflection of beams C1 and C2, which were strengthened with one layer and two layers of carbon FRP, respectively, are 1,206.3kN (271.4 kips) and 30.6mm (1.21 inch) and 1,432.0kN (322.2 kips) and 41.8mm (1.66 inch), respectively. The load-deflection curves of the beams in the G and GS-series showed similar behavior like the beams in the C-series. The shear strengths and the deflections corresponding to the peak loads of all 10 beams are given in detail in Table 3.

Figs. 7(a) and (b) show the maximum load and deflection versus the FRP ratio multiplied by its modulus of elasticity  $\rho_f E_f$ , respectively. The maximum load and deflection corresponding to the maximum load of all beams except beam C2 increase almost linearly with the increase of  $\rho_f E_f$ , regardless of fiber materials (carbon or glass) and configuration (continuous sheets or strips), while those of C2 do not because this beam failed in shear after flexural yielding.

### 5.2. Strain distributions of the FRP, the steel stirrups, and the LVDTs

The strain distributions of the FRP composites and steel stirrups just prior to shear failures of some beams (C1, G1, GS1, and GS5), which are considered to represent typical strain distributions of all specimens, are shown in Fig. 8. The figures also include the vertical strains measured by the LVDTs attached to the beams. Because the strain gages can measure only one point strain of stirrup or FRP sheet, the effective strains of FRP calculated by Eq.(10) were also compared with the average strains measured from LVDTs. In Fig. 8, the x-axis represents the location along the length of the beams (the distance to the section from the left support), while the y-axis represents the measured values of the strain gages or LVDTs. Almost all of the steel stirrups reached the yield strain before shear failure occurred, while the maximum strains of the FRP composites just prior to shear failures remained well below the rupture strains. The strains measured by the LVDTs were similar to those by the strain gages attached on the FRP.

Fig. 9 shows the effective strain at shear strength versus the FRP ratio multiplied by its modulus of elasticity  $\rho_f E_f$ . The strain in the transverse direction at the peak load tended to decrease as the amount of the FRP increased and as the spacing of the FRP strips decreased.

The strains in the transverse direction of all beams at the peak loads are presented in Table 3.

## 6. Comparison between the experimental and calculated results

### 6.1. Effective strain of the FRP

Fig. 10 shows the experimental and calculated effective strains of the FRP for the 9 test beams strengthened with FRP. The beam C2 that failed in shear after flexural yielding was excluded in the comparison. The open circles, in these figures, are the effective strains of the FRP measured using the LVDTs, while the open squares are the effective strains measured using the strain gages. The effective strains ( $\epsilon_{fe-ana}$ ) calculated according to Eq. (10) are also provided in the figure for comparison. The effective strains of FRP calculated by Eq.(10) were compared with the strains measured from both strain gages and LVDTs. The effective strain of the FRP decreases as the amount of FRP ( $\rho_f f_{fr}$ ) increases, and the effective strain predicted by the considered equation shows good agreement with the experimental results. The effective strain of the FRP ( $\epsilon_{fe-ana}$ ), the effective strength of concrete ( $v f_c'$ ), and the longitudinal strain ( $\epsilon_l$ ), of the 10 test beams calculated by the Eqs. (7), (9), and (10) are listed in Table 5. As the amount of FRP ( $\rho_f f_{fr}$ ) increases, the effective strain of the FRP decreases. Accordingly, the effective compressive strength of concrete and the longitudinal axial strain of the beam are correspondingly reduced due to the decrease in  $\epsilon_{fe}$ .

To further verify the applicability of the proposed method in predicting the effective strain of FRP, the predicted values of the proposed method were compared with the experimental results of FRP strengthened reinforced concrete beams [17, 19-22] reported in the technical

literature. Although there are abundant test results of load vs. deflection curves for RC beams strengthened with FRP, available test results of the effective strain of the FRP in RC beams, which failed due to crushing of concrete or FRP rupture without debonding (or premature failure/ peeling off), are limited. Thus, a total of 29 RC beams strengthened by FRP wrapping were compared in this study. All of the beams failed in shear due to crushing of the concrete or FRP rupture without debonding. The maximum compressive strength of concrete of the 29 beams was 40.5 MPa. All of the beams had a rectangular cross-section. It is reminded that the proposed method is capable of predicting the effective strain of the FRP in the RC beams that fail due to crushing of the concrete or FRP rupture without debonding (or premature failure/ peeling off). Thus the test results of the RC beams failed due to debonding were omitted in the comparison. The comparisons between the experimental and predicted results of the effective strains of the 29 beams are shown in Fig. 11 and summarized in Table 6. Fig. 11 compares the observed and predicted effective strains of the FRP. The predicted strains were calculated by Eq.(10). The mean and variance values of the effective strain ratio  $\varepsilon_{fe-test} / \varepsilon_{fe-ana}$  of the 29 RC beams as predicted by the proposed method are 1.00 and 16.2 %, respectively. The mean and variance values of the effective strain ratio  $\varepsilon_{fe-test} / \varepsilon_{fe-ana}$  of the 20 RC beams without the current beam tests were 0.94 and 14.35 %, respectively. The calculated effective strains by the existing equations in Table 1 were also compared with the observed ones as listed in Table 6. The variance values of  $\varepsilon_{fe-test} / \varepsilon_{fe-ana}$  as predicted by these equations were about 27.5%.

## 6.2. Shear strength of beams

Twenty two more RC beams [18, 23 & 24] reported in the technical literature were added to the 29 beams in Table 7 to check the applicability of the proposed equation based on the compatibility aided truss model in predicting the shear strength of the RC beams strengthened with FRP composites. Thus, total of 51 RC beams were compared with some of the existing models and the proposed equation. Four models are considered in this comparison: Chaallal *et al.*'s model [7], Triantafillou and Antonopoulos' model [8], Khalifa *et al.*'s model [9], and Chen and Teng's model [10]. These four models are chosen because, in authors' opinion, they represent a wide spectrum of prediction models available in the literatures.

All of the beams were reported to fail in shear without debonding (or premature failure/peeling off) before flexural yielding. The amount of the FRP composites ( $\rho_f f_{fr}$ ) varied from 0.33 MPa to 12.65 MPa. Three type of fiber materials (carbon, glass, and aramid) and two types of configuration (continuous sheets and strips) were used.

To define the shear strength of RC beams, the effective strain of the FRP,  $\varepsilon_{fe}$ , were calculated from the equations in Table 1 and Eq.(10). This will then allow the shear resistance contributions of FRP,  $V_f$ , to be determined using Eq. (2). Eq. (1) is then used to calculate the shear strength of RC beams,  $V_n$ . The shear strength,  $V_n$ , in Eq.(1) is influenced by not only

$V_f$  but also  $V_c$  and  $V_s$ . The shear equations of  $V_c$  and  $V_s$  in the design code (ACI 318-08 design code) were selected to calculate Eq.(1). No safety factors were considered in all shear strength calculations by the ACI 318-08 code. The angle of inclination of diagonal compressive stresses to the longitudinal axis of the member ( $\theta$ ) was assumed to be 45 degree in the calculation of  $V_s$  and  $V_f$ . The comparisons between the calculated and observed shear strength of the 51 beams are shown in Fig. 12 and summarized in Table 7.

Fig. 12 indicates the prediction results of each analytical model for varying  $\rho_f f_{fr} / f_c'$  on the shear strengths of the 51 RC beams. As can be seen from Fig. 12(a), the analytical result of Chaallal *et al.*'s model for the shear strength of 51 RC beams slightly overestimates with a mean  $V_{test} / V_{ana.}$  value of 0.93 and a COV (Coefficient of Variance) of 26.6%. As illustrated by Figs. 12 (b) and (c), the Triantafillou and Antonopoulos' model and Khalifa *et al.*'s model underestimated the observed shear strength of the 51 RC beams strengthened with FRP composites. The mean values of the shear strength ratios ( $V_{test} / V_{ana.}$ ) of the test beams calculated using Triantafillou and Antonopoulos' model and Khalifa *et al.*'s model are 1.78 and 1.24, with coefficient of variance values of 41.2% and 32.0%, respectively.

As shown in Fig. 12 (d), Chen and Teng's model underestimated the observed shear strength of the 51 RC beams, which derived the effective stress of FRP by using the stress distribution factor,  $D_{FRP}$  (ratio of the average strain to the maximum strain within the effective FRP height). It is noted that considering the simplicity of Chen and Teng's model,

this model predicted the shear strengths of 51 beams strengthened with FRP composites with reasonable agreement.

Fig. 12 (e) shows that the proposed solution method based on the smeared strains provides improved results compared to those obtained from the existing models for the different values of  $\rho_f f_{fr} / f_c'$  investigated in this research. It can be also seen from Fig. 10 (e), the numerical comparison of the proposed method indicates reasonable correlations with the experimental shear strength of the 51 RC beams with a mean of 1.04 and a COV of 20.6%. It is, therefore, worth noting that the compatibility aided truss model based on the average strains adopted in this study to calculate the effective strain of FRP is reasonably applicable to calculate the shear strengths of the RC beams strengthened with FRP composites. However, the validity of the proposed model needs to be verified against more independent experimental data, because the shear equations of  $V_c$  and  $V_s$  in the design code (ACI 318-08 design code) used to calculate Eq.(1) may not predict the exact shear resistance contributions of concrete and steel stirrups. Hence, the comparisons reported here are limited to those obtained from the current study. More elaborate comparisons with the test results of  $V_f$  are needed for future research.

## 7. Conclusions

The effective strain of the FRP plays an important role in predicting the shear strength of RC beams strengthened with FRP composites. In this paper, the effective strains of the FRP

used as strengthening material in RC beams were studied. Ten RC beams strengthened by FRP were tested and the strain of the FRP composites was measured at specified load intervals by the LVDTs attached to the beams and electrical strain gages installed on the surfaces of the FRP. The test results indicated that the effective strain of the FRP at shear failure decreased as the amount of FRP increased and also as the spacing of the FRP strips decreased.

An equation based on the compatibility-aided truss model was proposed to predict the effective strain of the FRP. The effective strain of the FRP calculated by the proposed equation depended on the interaction between the amount of FRP and the compressive strength of concrete. Even if the proposed Eq. (10a) was rather tedious to calculate the effective strain, this equation will help to understand the effects of the effective strength of concrete and the stress conditions of the materials of the beams at shear failure on the effective strain of the FRP. The obtained results showed that the proposed equation predicted the effective strains of the 29 FRP-strengthened RC beams with reasonable agreement. In addition, the numerical comparison of the proposed method indicates reasonable correlations with the experimental shear strength of the 51 RC beams with a mean of 1.04 and a COV of 20.6%.

The proposed method was capable of predicting the effective strain of the FRP in the RC beams that fail due to crushing of the concrete or FRP rupture without debonding. Thus

further rigorous research containing the effect of bond failure on the effective strain of the FRP composites is needed.

## References

- [1] Ceroni F, Pecce, M, Matthys S, Taerwe L. Debonding strength and anchorage devices for reinforced concrete elements strengthened with FRP sheets. *Compos Part B-Eng* 2008;39(3): 429-441.
- [2] Teng JG, Chen GM, Chen JF, Rosenboom OA, Lam L. Behavior of RC Beams Shear Strengthened with Bonded or Unbonded FRP Wraps. *J Compos Constr, ASCE*, 2009;15(5):394-404.
- [3] Deifalla A, Ghobarah A. Strengthening RC T-Beams Subjected to Combined Torsion and Shear Using FRP Fabrics: Experimental Study. *J Compos Constr, ASCE* 2009;15(3):301-411.
- [4] Grande E, Imbimb M, Rasulo A. Effect of Transverse Steel on the Response of RC Beams Strengthened in Shear by FRP: Experimental Study. *J Compos Constr, ASCE* 2009;15(5):405-414.
- [5] Fico R, Prota A, Manfredi G. Assessment of Eurocode-like design equations for the shear capacity of FRP RC members. *Compos Part B-Eng* 2008;39(5):792-806.
- [6] Li A, Diagana C, Delmas Y. "Shear strengthening effect by bonded composite fabrics on RC beams. *Compos Part B-Eng* 2002;33(3):225-239.
- [7] Chaallal O, Nollet MJ, Perration D. Strengthening of Reinforced Concrete Beams with Externally Bonded Fibre-Reinforced-Plastic Plates. *Canadian J Civil Eng* 1998;25(4): 692-704.
- [8] Triantafillou TC, Antonopoulos C. Design of Concrete Flexural Members Strengthened in Shear with FRP. *J Compos Constr, ASCE*, 2000;4(4):198-205.
- [9] Khalifa A, Gold WJ, Nanni A, Aziz A. Contribution of Externally Bonded FRP to Shear Capacity of RC Flexural Members. *J Compos Constr, ASCE* 1998;2(4):195-203.
- [10] Chen JF, Teng JG. Shear Capacity of Fiber-Reinforced Polymer-Strengthened Reinforced Concrete Beams: Fiber Reinforced Polymer Rupture", *J Struct Eng* 2003; 129(5):615-625.
- [11] Lee JY, Kim SW. Torsional Strength of Reinforced Concrete Beams Considering Tension Stiffening Effect", *J Struct Eng, ASCE* 2010;136(11)(to be issued).
- [12] Vecchio F, Collins MP. The Modified Compression-Field Theory for RC Elements

- Subjected to Shear. ACI Struct J 1986; 83(2):219-231.
- [13] Lee JY, and Watanabe F. Shear Design of RC Beams with Shear Reinforcement Considering Failure Modes. ACI Struct J 2000; 97(3):477-484.
- [14] Mohamad YM, Lee JY, Hsu TTC. Cyclic Stress-Strain Curves of Concrete and Steel Bars in Membrane Elements. J Struct Eng 2001;127(12):1402-1411.
- [15] Vecchio FJ, Collins MP. Predicting the Response of RC Beams Subjected to Shear Using the Modified Compression Field Theory. ACI Struct J 1988;85(4):258-268.
- [16] Watanabe F, Lee JY. Theoretical Prediction of Shear Strength and Failure Mode of Reinforced Concrete Beams. ACI Struct J 1998; 95(6):749-757.
- [17] Ohuchi H, Ohno S, Katsumata H. Seismic strengthening design technique for existing bridge columns with CFRP. Proceedings of the 2nd International Workshop on Seismic Design and Retrofitting of Reinforced Concrete Bridges, R. Park, Ed., 1994:495-514, Queenstown, New Zealand.
- [18] Araki N, Matsuzaki Y, Nakano K, Kataoka T. Experimental Study on Shear Capacity of RC Beams using Sheet Type Fiber. Proceedings of the JCI 1997;19(2):207-212.
- [19] Uji K. Improving the shear capacity of existing reinforced concrete members by applying carbon fiber sheets. Trans. Japan concrete Institute 1992;14:253-266.
- [20] Miyauchi K, Inoue S, Nishibayashi S, Tanaka Y. Shear behavior of RC beam strengthened with CFRP sheet. Trans. Japan concrete Institute 1997;19:97-104.
- [21] Funakawa I, Shimono K, Watanabe T, Asada S, Ushijima S. Experimental study on shear strengthening with continuous fiber reinforcement sheet and methyl methacrylate resin. Non-Metallic (FRP) Reinforcement for Concrete Structures, Proceeding of the Third International Symposium, Sapporo, Japan, 1997. p. 475-482.
- [22] Umezu K, Fujita M, Nakai H, Tamaki K. Shear behavior of RC beams with aramid fiber sheet. Non-Metallic (FRP) Reinforcement for Concrete Structures, Proceeding of the Third International Symposium, Sapporo, Japan, 1997. p. 491-498.
- [23] Kato H, Kojima T, Takagi N, Hamada Y. Experimental Study on Shear Reinforcement of RC Beams by using Carbon Fiber Sheets. Proceedings of the JCI 1996;18(2):101-106.
- [24] Ishizaki K, Maruyama Y, Nakano K, Kataoka T. Size Effect in Shear Strength of RC Beams Retrofitted with CFRP Sheet. Proceedings of the JCI 1997;19(2): 201-206.

**Table 1**

Various equations for the effective strain of FRP.

Reference	$\varepsilon_{fe}$	Note
<b>Chaallal et al.</b> <sup>7)</sup>	$0.8 \varepsilon_{fu}$	-
<b>Triantafillou and Antonopoulos</b> <sup>8)</sup>	$0.17 \left( \frac{(f_c')^{2/3}}{E_f \rho_f} \right)^{0.30} \varepsilon_{fu}$	For fully wrapped CFRP (CFRP fracture)
	$0.048 \left( \frac{(f_c')^{2/3}}{E_f \rho_f} \right)^{0.47} \varepsilon_{fu}$	For fully wrapped AFRP (AFRP fracture)
<b>Khalifa et al.</b> <sup>9)</sup>	$(0.5622(\rho_f E_f)^2 - 1.2188\rho_f E_f + 0.778)\varepsilon_{fu} \leq 0.5\varepsilon_{fu}$	-
<b>Chen and Teng</b> <sup>10)</sup>	$(1 + \zeta) / 2$ where $\zeta = z_t / z_b$ , $z_t = d_{FRP,t}$ , $z_b = 0.9d$	For FRP rupture failure

**Table 2**

Material properties and calculated results of analyzed three beams.

Beams	$f_c'$ (MPa)	Shear steel reinforcement			Longitudinal tensile reinforcement		FRP composites				Balanced FRP ratio by Eq. (4)	Effective strain	Failure mode
		$\rho_t$ (%)	$f_{ty}$ (MPa)	$\beta$ (Deg)	$\rho_t$ (%)	$f_{ty}$ (MPa)	$f_{fr}$ (MPa)	$\varepsilon_{fr}$ (%)	$E_f$ (GPa)	$\rho_f$ (%)			
B1	40.0	0.10	300.0	90.0	2.00	550.0	3,825.0	1.53	250.0	<b>0.0244</b>	<b>0.0244</b>	<b>1.53</b>	<b>Balanced failure</b>
B2	40.0	0.10	300.0	90.0	2.00	550.0	3,825.0	1.53	250.0	<b>0.08</b>	<b>0.0244</b>	<b>1.00</b>	<b>Mode 1</b>
B3	40.0	0.10	300.0	90.0	2.00	550.0	3,825.0	1.53	250.0	<b>0.16</b>	<b>0.0244</b>	<b>0.77</b>	<b>Mode 1</b>

(Note: 1 MPa = 145 psi)

**Table 3**

Specification of specimens and test results.

Series	Beams	Fiber	FRP composites				$\rho_f E_f$ (MPa)	$P_n$ (kN)	$\Delta_n$ (mm)	F. M.	Vertical strains (%)		
			Distribution	$s_f$ (mm)	$n_f$	$\rho_f$ (%)					$\varepsilon_{fe-LVDT}$	$\varepsilon_{fe-frp}$	$\varepsilon_{se-steel}$
C	C1	Carbon	sheets	-	1	0.063					0.775	0.923	0.956
	C2	Carbon	sheets	-	2	0.126	157.5	1206.3	30.6	S	0.614	0.747	2.045
G	G1	Glass	sheets	-	1	0.286	315.0	1432.0	41.8	F	1.193	1.452	0.990
	G2	Glass	sheets	-	2	0.572	48.6	938.0	18.5	S	0.877	1.282	1.557
	G3	Glass	sheets	-	3	0.858	97.2	1103.0	26.5	S	1.000	1.172	1.026
	G4	Glass	sheets	-	4	1.144	145.9	1162.5	32.0	S	1.012	1.094	1.226
GS	GS1	Glass	strips	300	1	0.095	194.5	1379.0	45.3	S	1.728	1.533	2.148
	GS1a	Glass	strips	200	1	0.143	16.2	639.0	14.0	S	1.589	1.633	1.597
	GS3	Glass	strips	200	3	0.429	24.3	712.5	14.3	S	1.225	1.316	1.242
	GS5	Glass	strips	200	5	0.714	72.9	855.0	19.0	S	0.989	1.196	2.521

(Note: 1 MPa = 145 psi; ; 1 kN = 0.225 kip; 1mm = 0.0394 in.)

Note:  $s_f$  is the spacing of FRP strips,  $n_f$  is the number of FRP layers;  $\rho_f$  is the ratio of FRP, F.M.: failure mode,  $P_n$  is the maximum load;  $\Delta_n$  is the midspan deflection corresponding to  $P_n$ ;  $\varepsilon_{fe-LVDT}$  is the strain measured using the vertical LVDT;  $\varepsilon_{fe-frp}$  and  $\varepsilon_{fe-steel}$  are the strains measured using the strain gage attached on the FRP and the steel stirrups, respectively; F.M.: failure modes; S : shear failure due to concrete crushing before yielding of the flexural steel; F : shear failure after yielding of the flexural steel.

**Table 4**

Material properties of steel rebars and FRPs.

Materials	Section area (mm <sup>2</sup> )	$t_f$ (mm)	$\varepsilon_y$ or $\varepsilon_{fr}$	$f_y$ or $f_{fr}$ (MPa)	$E_s$ or $E_f$ (MPa)
D10 (Stirrups)	71.3	-	0.0017	300	180,000
D25 (Long. Reinforcement)	506.7	-	0.0028	525	190,000
Carbon FRP (Shear reinforcement)	-	0.11	0.0180	4,510	250,000
Glass FRP (Shear reinforcement)	-	0.50	0.0200	350	17,000

$t_f$  is the thickness of FRP,  $\varepsilon_{fr}$  and  $\varepsilon_y$  are the rupture strain of FRP and yield strain of steel bars, respectively,  $f_{fr}$  and  $f_y$  are the rupture strength of FRP and yield strength of FRP bars, respectively,  $E_f$  and  $E_s$  are the modulus of elasticity of FRP and steel bars, respectively.

(Note: 1 MPa = 145 psi; 1mm = 0.0394 in.)

**Table 5**

Experimental and calculated results of the 10 test beams.

Series	Beams	$\frac{\rho_f f_{fr}}{f_c'}$	Analytical results			Test results		$\frac{\varepsilon_{fe-LVDT}}{\varepsilon_{fe-ana}}$	$\frac{\varepsilon_{fe-frp}}{\varepsilon_{fe-ana}}$
			$\nu f_c'$ (MPa)	$\varepsilon_l$	$\varepsilon_{fe-ana}$	$\varepsilon_{fe-LVDT}$	$\varepsilon_{fe-frp}$		
C	C1	0.081	13.39	0.00163	0.00801	0.00775	0.00923	0.85730	1.0210
	C2	0.162	15.02	0.00174	0.00634	0.00614	0.00747	0.84573*	1.0289*
G	G1	0.029	11.29	0.00145	0.01074	0.01193	0.01452	0.98758	1.2020
	G2	0.057	12.43	0.00155	0.00901	0.00877	0.01282	0.85063	1.2435
	G3	0.086	13.23	0.00162	0.00800	0.01000	0.01172	1.0823	1.2684
	G4	0.114	13.86	0.00166	0.00730	0.0101	0.01094	1.1896	1.2886
GS	GS1	0.009	10.10	0.00133	0.01311	0.01728	0.01533	1.2033	1.0675
	GS1a	0.014	10.46	0.00136	0.01232	0.01589	0.01633	1.1667	1.1990
	GS3	0.029	11.29	0.00145	0.01074	0.01225	0.01316	1.0141	1.0894
	GS5	0.043	11.92	0.00151	0.00974	0.00989	0.01196	0.89421	1.0814
Ave.								1.03	1.16
V. C.								13.73 %	8.47 %

$\varepsilon_{fe-ana}$  is the effective strain of the FRP calculated by the proposed method; Ave. is the mean value; V.C is the variance coefficient. \* C2 failed in shear after flexural yielding. (Note: 1 MPa = 145 psi)

**Table 6**

Experimental and calculated effective strains of FRP in RC beams.

Beams	$\varepsilon_{fe-test}$ (%)	*1	*2	*3	*4	*5	Beams	$\varepsilon_{fe-test}$ (%)	*1	*2	*3	*4	*5
3 <sup>19)</sup>	0.50	0.54	1.06	1.26	1.09	0.83	AN-1/5 Z-3 <sup>20)</sup>	1.25	1.03	1.12	1.66	2.08	1.04
BS12 <sup>17)</sup>	0.84	0.87	1.44	1.44	1.75	1.03	AN-1/2 Z-3 <sup>20)</sup>	0.79	0.65	0.94	1.04	1.31	0.94
BS24 <sup>17)</sup>	0.62	0.65	1.31	1.87	1.29	1.02	CN-1/L Z-2 <sup>20)</sup>	0.92	0.76	1.07	1.22	1.53	0.87
BM06 <sup>17)</sup>	1.17	1.22	1.63	1.95	2.44	1.10	S-2 <sup>21)</sup>	0.65	0.51	0.66	0.81	1.08	0.74
BM12 <sup>17)</sup>	0.93	0.97	1.59	1.60	1.94	1.14	S-4 <sup>21)</sup>	0.44	0.34	0.62	0.72	0.73	0.72
BM18 <sup>17)</sup>	0.78	0.81	1.51	1.76	1.62	1.13	CS2 <sup>22)</sup>	0.80	0.57	0.62	0.91	1.33	0.66
BM24 <sup>17)</sup>	0.60	0.62	1.27	1.81	1.25	0.98	C1	0.92	0.64	0.85	1.03	1.54	1.02
BL06 <sup>17)</sup>	0.84	0.87	1.17	1.40	1.75	0.79	G1	1.45	0.91	0.85	1.45	2.42	1.20
BL12 <sup>17)</sup>	0.78	0.81	1.34	1.34	1.62	0.96	G2	1.28	0.80	0.92	1.28	2.14	1.24
BMW06 <sup>17)</sup>	0.84	0.87	1.24	1.40	1.75	0.93	G3	1.17	0.73	0.95	1.17	1.95	1.27
BMW012 <sup>17)</sup>	0.69	0.72	1.25	1.19	1.44	1.00	G4	1.09	0.68	0.97	1.09	1.82	1.29
BMW24 <sup>17)</sup>	0.46	0.48	1.03	1.39	0.96	0.90	GS1	1.53	0.96	0.64	1.53	2.56	1.07
2 <sup>17)</sup>	1.20	1.25	1.34	2.00	2.50	1.00	GS1a	1.63	1.02	0.77	1.63	2.72	1.20
3 <sup>17)</sup>	1.03	1.07	1.42	1.72	2.15	0.96	GS3	1.32	0.82	0.77	1.32	2.19	1.09
							GS5	1.20	0.75	0.79	1.20	1.99	1.08
Ave.									0.78	1.06	1.37	1.74	1.00
V. C.(%)									27.6	28.0	24.5	29.5	16.2

$$*1 = \varepsilon_{fe-test} / \varepsilon_{fe-chaallal}^{7)}, *2 = \varepsilon_{fe-test} / \varepsilon_{fe-Tri\&Anto}^{8)}, *3 = \varepsilon_{fe-test} / \varepsilon_{fe-Khalifa}^{9)},$$

$$*4 = \varepsilon_{fe-test} / \varepsilon_{fe-Chen\&Teng}^{10)}, *5 = \varepsilon_{fe-test} / \varepsilon_{fe-Eq.(10)}$$

**Table 7**

Experimental and calculated shear strengths of RC beams.

Beams	$V_{n-exp.}$ (kN)	*1	*2	*3	*4	*5	Beams	$V_{n-exp.}$ (kN)	*1	*2	*3	*4	*5
3 <sup>19)</sup>	59.5	0.77	0.59	1.78	1.02	0.95	N-E100Z*2 <sup>23)</sup>	132	1.28	1.42	2.45	1.79	1.87
BS12 <sup>17)</sup>	310	1.37	1.19	3.20	1.69	1.86	N-E100*2 <sup>23)</sup>	183	1.13	1.3	3.34	2.44	1.99
BS24 <sup>17)</sup>	396	1.34	0.92	3.96	2.02	1.62	N-E100S <sup>23)</sup>	103	0.96	1.07	1.91	1.39	1.43
BM06 <sup>17)</sup>	192	0.99	1.00	1.72	1.24	1.32	N10-E100S <sup>23)</sup>	139	0.92	0.99	1.42	1.17	1.20
BM12 <sup>17)</sup>	264	1.09	0.95	2.32	1.32	1.44	RB-CF-45 <sup>18)</sup>	241	1.18	1.09	1.45	1.24	1.3
BM18 <sup>17)</sup>	315	1.12	0.87	2.72	1.48	1.42	RB-CF-64 <sup>18)</sup>	267	1.18	1.01	1.59	1.22	1.32
BM24 <sup>17)</sup>	325	1.04	0.72	2.77	1.52	1.25	RB-CF-97 <sup>18)</sup>	313	1.22	0.93	1.83	1.2	1.34
BL06 <sup>17)</sup>	169	0.80	0.81	1.31	0.98	1.04	RB-CF-131 <sup>18)</sup>	365	1.28	0.88	2.11	1.21	1.38
BL12 <sup>17)</sup>	250	0.96	0.85	1.91	1.15	1.25	RB-CF-243 <sup>18)</sup>	415	1.17	0.62	2.33	1.28	1.13
BMW06 <sup>17)</sup>	181	1.04	0.98	1.74	1.23	1.31	RB-AF-60 <sup>18)</sup>	242	1.22	0.94	1.41	1.12	1.34
BMW012 <sup>17)</sup>	239	1.12	0.88	2.26	1.24	1.36	RB-AF-90 <sup>18)</sup>	264	1.22	0.82	1.51	1.04	1.36
BMW24 <sup>17)</sup>	293	1.08	0.66	2.69	1.42	1.16	RB-AF-120 <sup>18)</sup>	318	1.36	0.81	1.79	1.09	1.52
2 <sup>17)</sup>	430	1.08	1.14	1.45	1.27	1.31	No.2 <sup>24)</sup>	285	1.08	1.14	1.44	1.27	1.32
3 <sup>17)</sup>	530	1.14	1.15	1.77	1.37	1.44	No.3 <sup>24)</sup>	236	0.98	0.93	1.18	1.04	1.15
AN-1/5 Z-3 <sup>20)</sup>	75.2	0.82	0.82	1.03	0.91	0.94	No.7 <sup>24)</sup>	569	1.03	1.10	1.45	1.25	1.31
AN-1/2 Z-3 <sup>20)</sup>	86	0.82	0.71	1.17	0.87	0.92	No.8 <sup>24)</sup>	530	1.03	1.00	1.33	1.15	1.30
CN-1/L Z-2 <sup>20)</sup>	93.1	1.11	1.04	2.18	1.37	1.50	C1	603	0.89	0.76	1.2	0.91	1.00
S-2 <sup>21)</sup>	691	0.55	0.49	0.75	0.58	0.62	G1	469	0.83	0.79	0.95	0.86	0.9
S-4 <sup>21)</sup>	942	0.57	0.38	0.99	0.60	0.61	G2	551	0.89	0.79	1.1	0.91	0.99
N-E100Z <sup>23)</sup>	103	1.32	1.41	1.93	1.61	1.68	G3	581	0.87	0.72	1.15	0.87	0.98
N-E100 <sup>23)</sup>	160	1.49	1.66	2.97	2.15	2.22	G4	689	0.97	0.75	1.36	0.95	1.10
N10-E100 <sup>23)</sup>	169	1.11	1.20	1.72	1.42	1.45	GS1	319	0.62	0.62	0.65	0.63	0.64
N-E200 <sup>23)</sup>	165	1.01	1.17	3.01	2.20	1.80	GS1a	356	0.67	0.66	0.73	0.69	0.71
N10-E200 <sup>23)</sup>	201	1.05	1.09	2.03	1.69	1.48	GS3	427	0.76	0.72	0.86	0.79	0.82
N-H100 <sup>23)</sup>	149	1.4	1.26	2.68	1.66	1.82	GS5	513	0.86	0.80	1.03	0.89	0.95
N10-H100 <sup>23)</sup>	169	1.23	1.04	1.69	1.26	1.34							
Ave.									0.93	1.78	1.24	1.28	1.04
V. C.(%)									26.6	41.2	32.0	26.9	20.6

$$*1=V_{n-exp.}/V_{n-chaallal}^{7)}, *2=V_{n-exp.}/V_{n-Tri\&Anto}^{8)}, *3=V_{n-exp.}/V_{n-Khalifa}^{9)}, *4=V_{n-exp.}/V_{n-Chen\&Teng}^{10)},$$

$$*5=V_{n-exp.}/V_{n-Eq.(1)}$$

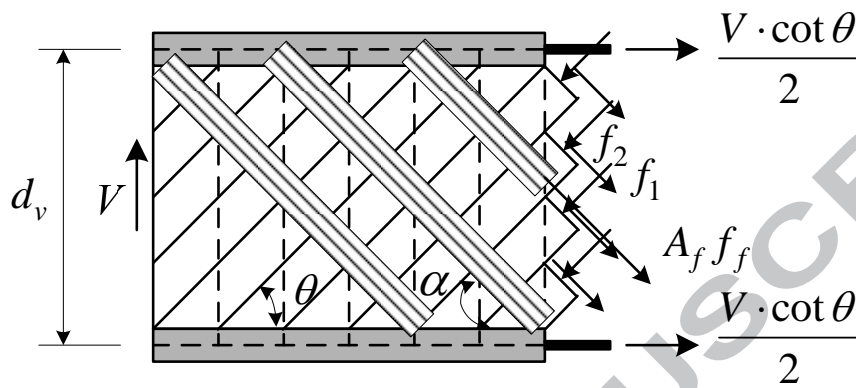


Fig. 1 A truss model of a FRP strengthened RC beam.

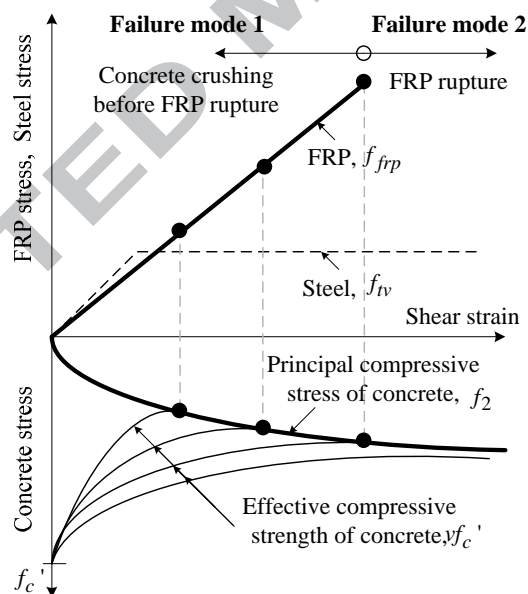
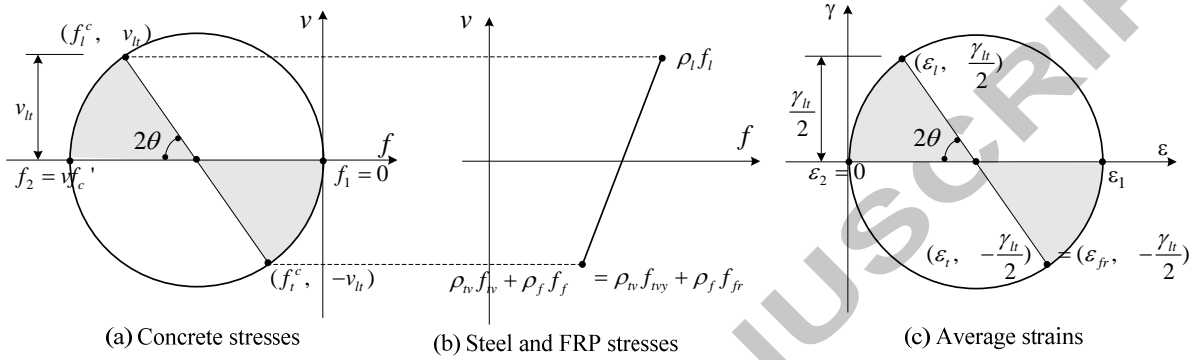
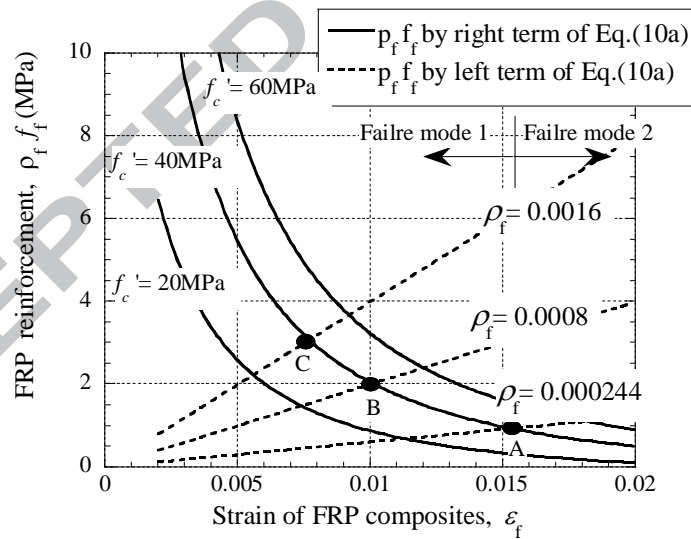


Fig. 2. Stresses of materials versus strain of RC beams strengthened with FRP composites.



**Fig. 3.** Mohr's stress and strain circles at the boundary between failure mode 1 and failure mode 2.



**Fig. 4.** Calculation of the effective strain of FRP composites at shear failure. (Note: 1 MPa = 145 psi)

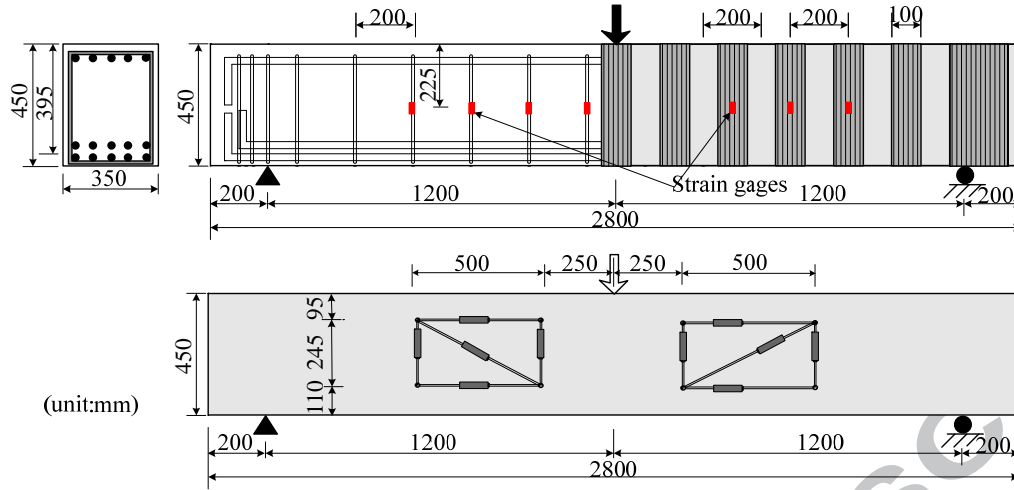


Fig. 5. Dimensions and reinforcement of test beams of GS-series. (Note: 1mm = 0.0394 in.)

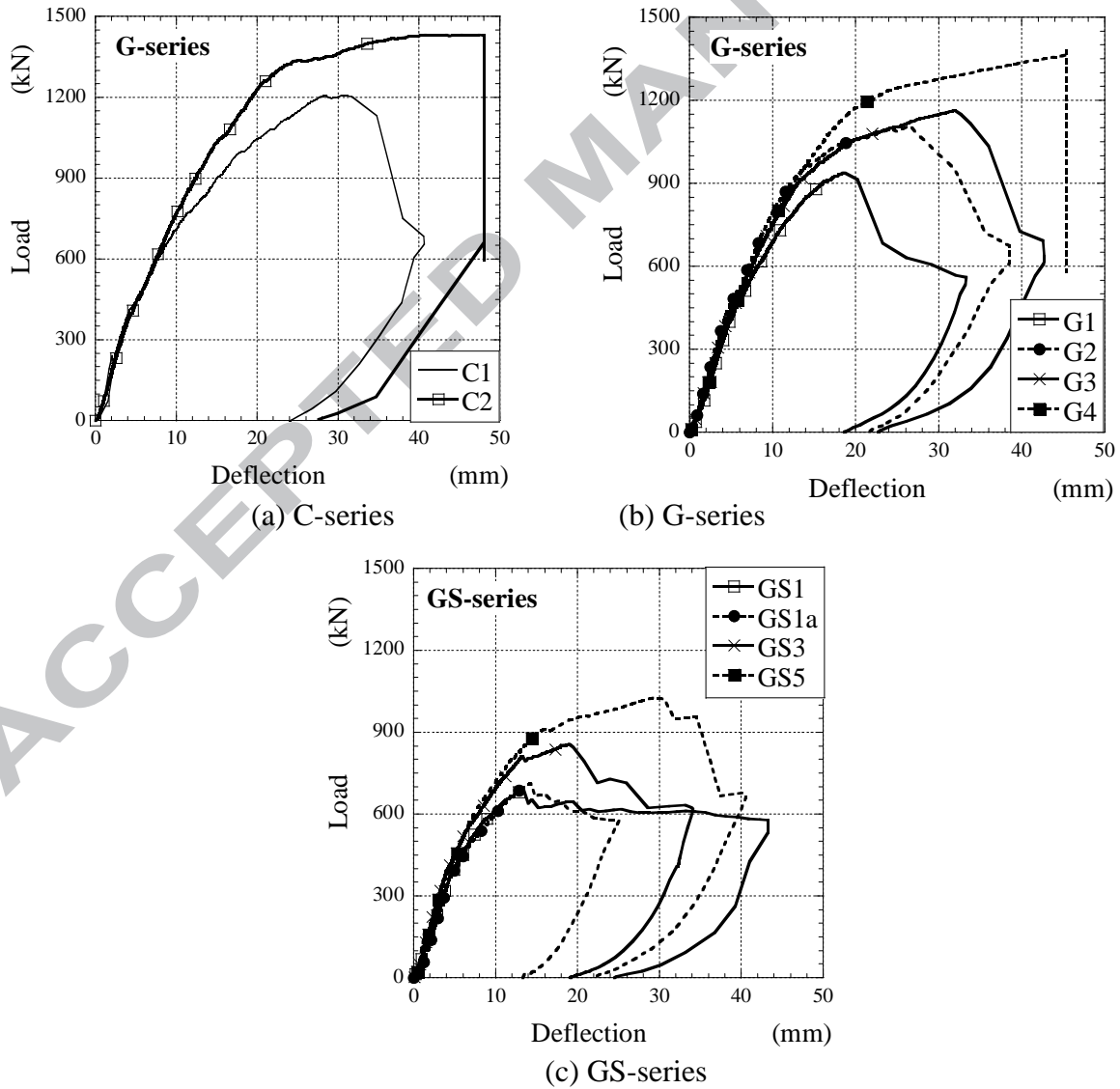
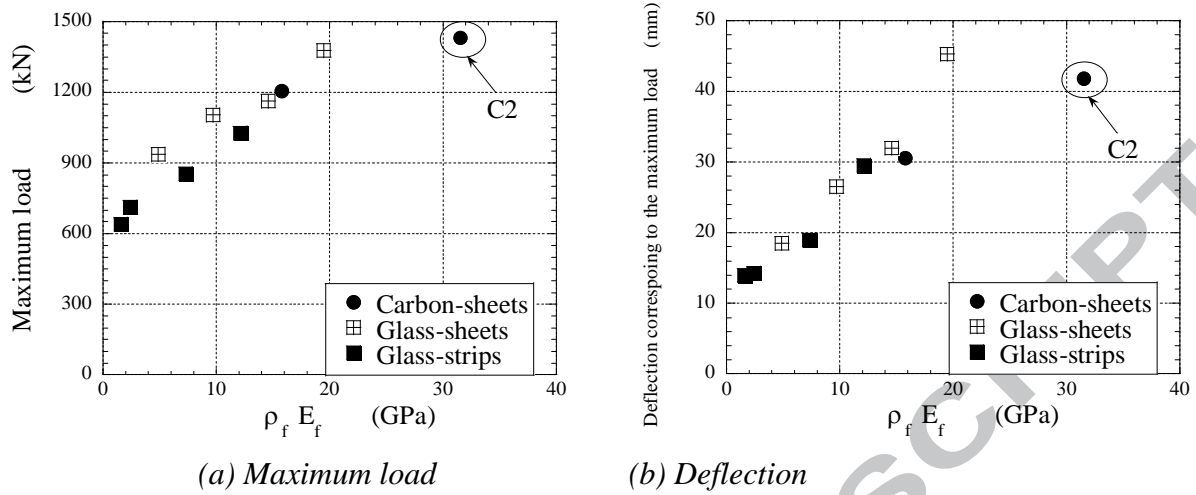


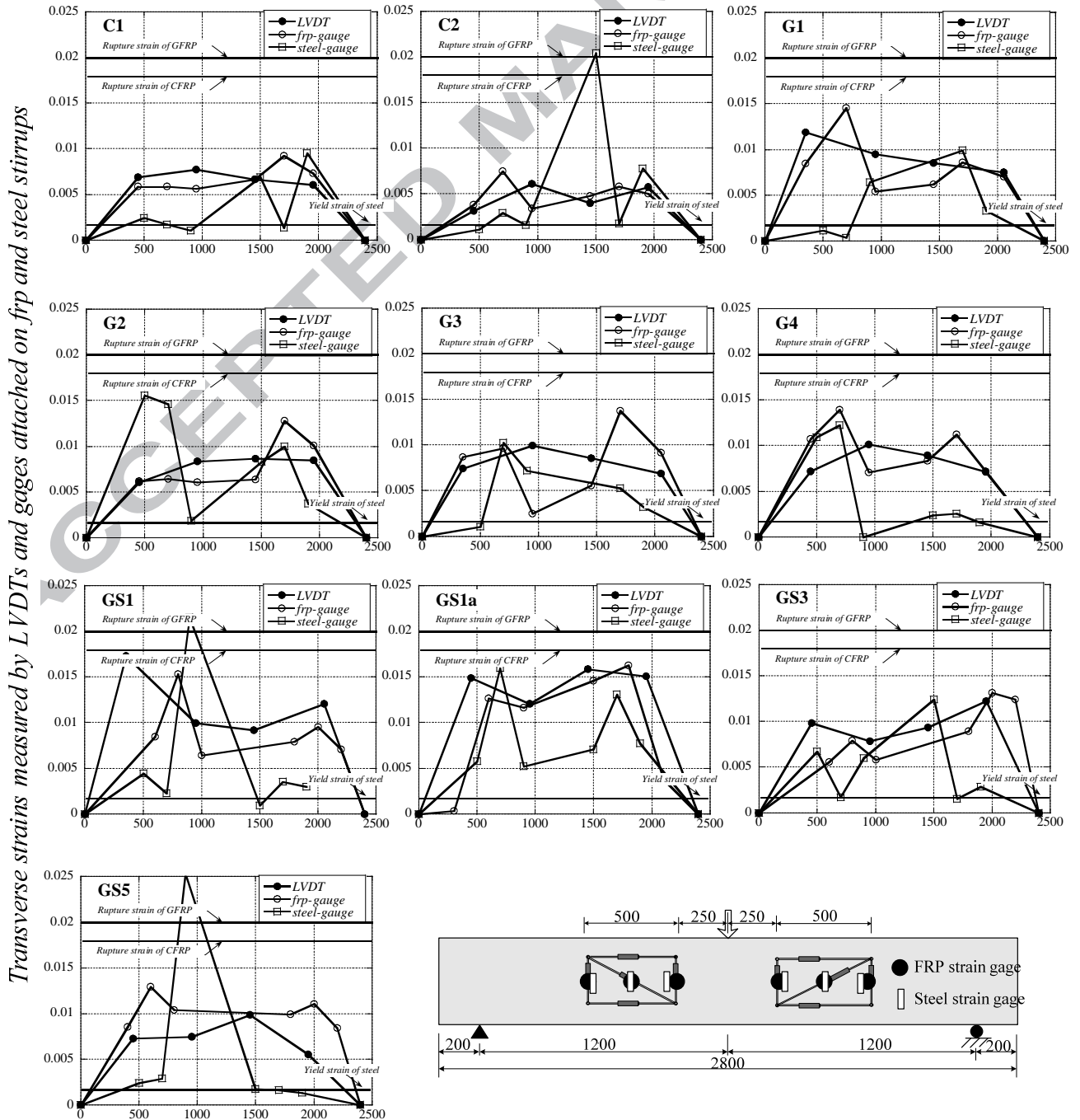
Fig. 6. Load versus deflection curves of the test beams. (Note: 1 kN = 0.225 kip; 1mm = 0.0394 in.)



(a) Maximum load (b) Deflection

Fig. 7. Maximum load and deflection of the test beams.

(Note: 1 GPa = 145 ksi; 1mm = 0.0394 in.)



Transverse strains measured by LVDTs and gages attached on FRP and steel stirrups

Locations of LVDTs and gages attached on FRP and steel stirrups

**Fig. 8.** Strain distributions of the FRP, the steel stirrups, and the LVDTs.

(Note: 1mm = 0.0394 in.)

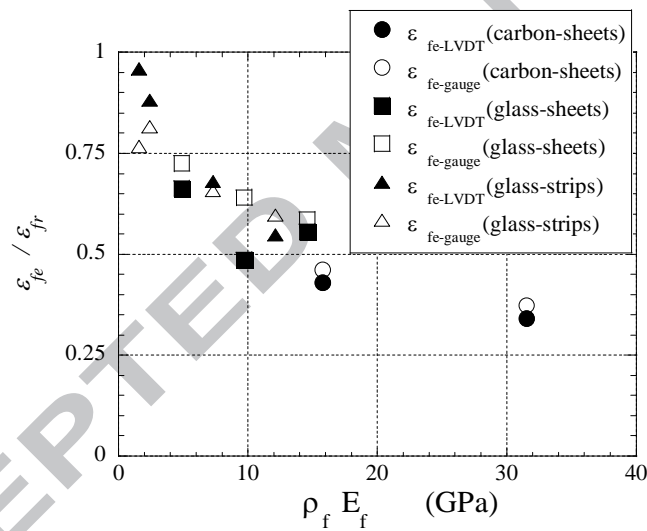


**Fig. 9.** Effective strain of the test beams at shear strength. (Note: 1 GPa = 145 ksi)

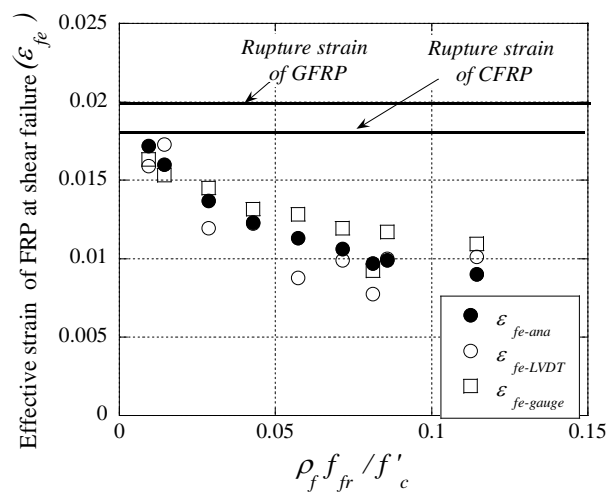


**Fig. 10.** Comparison between the experimental and calculated effective strains of FRP in 9 test beams.

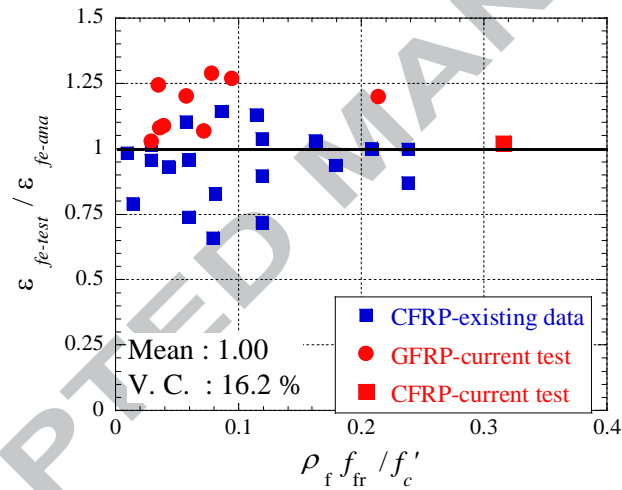


**Fig. 11.** Comparison between the experimental and calculated effective strains of FRP in RC beams reported in the technical literature.

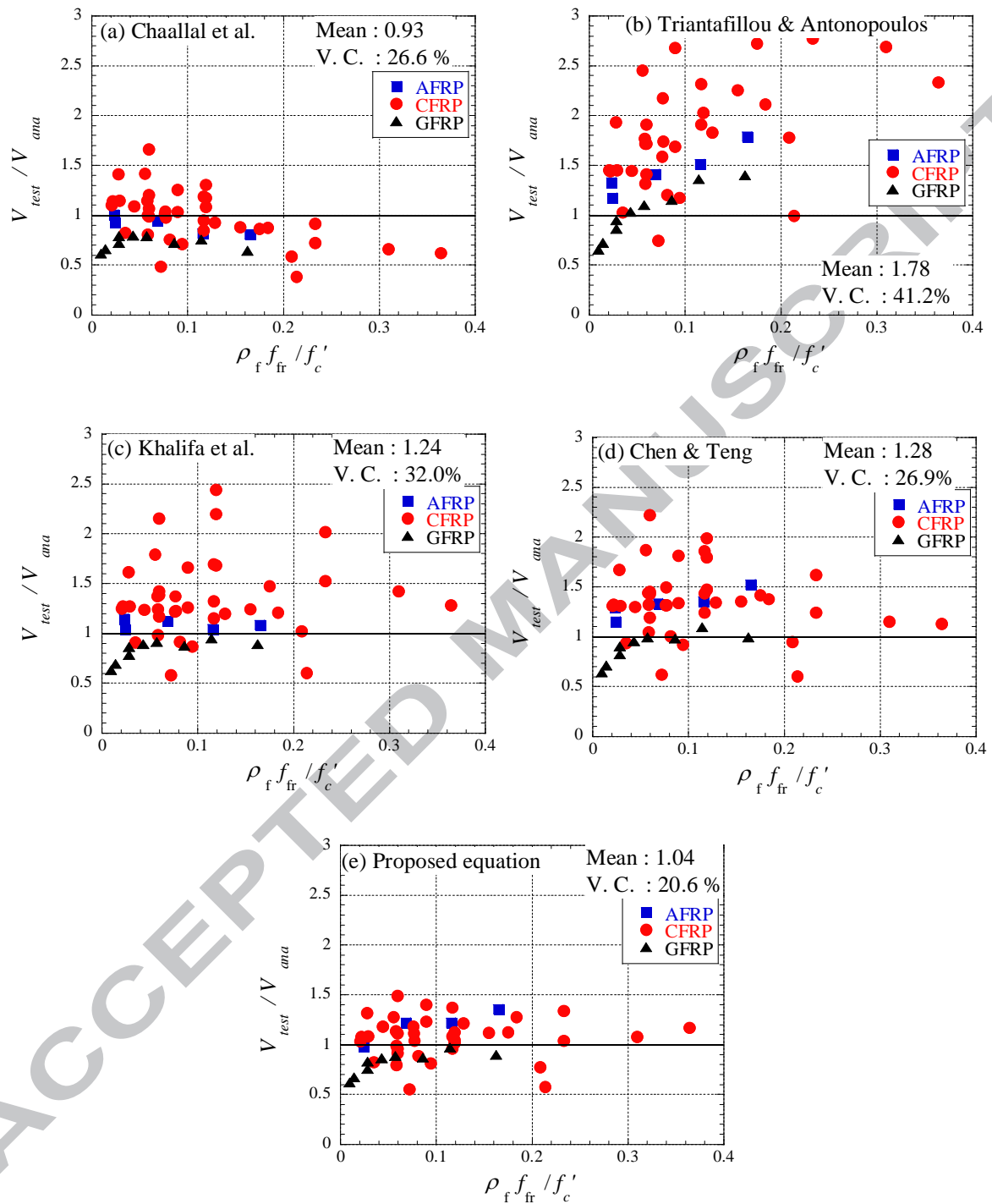


**Fig. 12.** Comparison between the experimental and calculated shear strengths RC beams strengthened with FRP composites reported in the technical literature.